

Polycyclic aromatic hydrocarbons in the dwarf galaxy IC 10

Wiebe D.S.¹, Egorov O.V.², Lozinskaya T.A.²

May 29, 2022

¹*Institute of Astronomy, Russian Academy of Sciences, ul. Pyatnitskaya 48, Moscow, 119017 Russia*

²*Sternberg Astronomical Institute, Universitetskii pr. 13, Moscow, 119992 Russia*

Abstract

Infrared observation from the Spitzer Space Telescope archive are used to study the dust component of the interstellar medium in the IC 10 irregular galaxy. Dust distribution in the galaxy is compared to the distributions of H α and [SII] emission, neutral hydrogen and CO clouds, and ionizing radiation sources. The distribution of polycyclic aromatic hydrocarbons (PAH) in the galaxy is shown to be highly non-uniform with the mass fraction of these particles in the total dust mass reaching 4%. PAHs tend to avoid bright HII regions and correlate well with atomic and molecular gas. This pattern suggests that PAHs form in the dense interstellar gas. We propose that the significant decrease of the PAH abundance at low metallicity is observed not only globally (at the level of entire galaxies), but also locally (at least, at the level of individual HII regions). We compare the distribution of the PAH mass fraction to the distribution of high-velocity features, that we have detected earlier in wings of H α and SII lines, over the entire available galaxy area. No conclusive evidence for shock destruction of PAHs in the IC 10 galaxy could be found.

1 Introduction

Numerous infrared space observatories, first of all, the Spitzer space telescope, as well as MSX and ISO satellites, opened up a new era in studies

of the star formation both in nearby and distant galaxies. The so-called polycyclic aromatic hydrocarbons (PAH) [1] — macromolecules consisting of several tens or several hundred atoms, mostly carbon and hydrogen — are of special interest in relation to these observations. The absorption of an ultraviolet (UV) photon by such a molecule excites bending and vibrational modes, and, as a result, near IR photons are emitted. PAH emission bands may account for a substantial fraction (up to several dozen percent) of the entire infrared luminosity of the galaxy [2].

Polycyclic aromatic hydrocarbons attract considerable interest at least for two reasons. First, their emission is related to the overall UV radiation field of a galaxy, making them a natural indicator of the star formation rate. Second, PAH molecules not only trace the state of the interstellar medium, but also play an important role in its physical and chemical evolution. The former aspect is interesting both for interpretation of available IR observations and for planning new near-IR space missions (JWST, SOFIA, SPICA, etc.). The latter aspect is of great importance for development of models for various objects ranging from protoplanetary disks to the interstellar medium of an entire galaxy.

Unfortunately, PAH formation and destruction mechanisms in the interstellar medium still are not understood. Such possible scenarios as the synthesis of PAHs in carbon-rich atmospheres of AGB and post-AGB stars or in dense molecular clouds as well as the destruction of PAHs by shocks and UV radiation are discussed extensively in the literature (see Sandstrom et al. [3] and references therein). The observed deficit of the emission of these macromolecules in metal-poor galaxies may be an important indication of the nature of the PAH evolutionary cycle. Note that, as shown by Draine et al. [4], this deficit is related to the real lack of PAHs and not to the low efficiency of the excitation of their IR transitions. In galaxies with oxygen abundance $12 + \log(\text{O}/\text{H}) > 8.1$ the typical mass fraction of PAHs q_{PAH} (the fraction of the total dust mass in particles consisting of at most one thousand atoms) is equal to about 4%, i.e., about the same as in the Milky Way. At metallicities $12 + \log(\text{O}/\text{H}) < 8.1$ the average q_{PAH} decreases quite sharply down to 1% and even lower.

In order to clarify the cause of this transition and to identify the PAH formation and destruction mechanisms as well as their relation to the physical parameters and the metallicity of a galaxy, Sandstrom et al. [3] analyzed in detail Spitzer observations of the dust component in the nearest irregular dwarf galaxy — the Small Magellanic Cloud (SMC). These authors found

weak correlation or no correlation between q_{PAH} and such SMC parameters as the location of carbon-rich asymptotic giant branch stars, supergiant HI shells and young supernova remnants, and the turbulent Mach number. They showed that q_{PAH} correlates with CO intensity and increases in regions of high dust and molecular gas surface density. Sandstrom et al. [3] concluded that PAH mass fraction is high in regions of active star formation, but suppressed in bright HII regions.

The irregular dwarf galaxy IC 10 is analogous to the SMC in terms of a number of parameters. The average gas metallicity in IC 10 is $12 + \log(\text{O}/\text{H}) \simeq 8.2$, varying from 7.6 to 8.5 in different HII regions ([5, 6, 7] and references therein), i.e., it covers the very range where the transition from high to low PAH abundance occurs.

The interstellar medium of this galaxy is characterized by a filamentary, multi-shell structure. In $\text{H}\alpha$ and [SII] images IC 10 appears as a giant complex of multiple shells and supershells, arc- and ring-shaped features with sizes ranging from 50 to 800–1000 pc (see [8, 9, 10, 11, 12] and references therein). The HI distribution also shows numerous “holes”, supershells, and extended irregular features with rudiments of a spiral pattern [8].

The IC 10 galaxy is especially attractive for the analysis of the dust component because, unlike the SMC, it is a starburst galaxy. It is often classified as a BCD-type object because of its high $\text{H}\alpha$ and IR luminosity [13]. The stellar population of IC 10 shows evidence of two star formation bursts. The first burst is at least 350 Myr old, while the second one has occurred 4–10 million years ago (see [14, 15, 16] and references therein). For the purpose of identifying the influence of shocks and/or UV radiation on dust the anomalously large population of Wolf–Rayet (WR) stars in IC 10 is of special interest. Here the highest density of WR stars is observed among the known dwarf galaxies, comparable to the density of these stars in massive spiral galaxies [13, 15, 16, 17, 18, 19]. High $\text{H}\alpha$ and IR luminosity of IC 10, combined with the large number of WR stars, indicates that the last burst of star formation in this galaxy must have been short, but engulfed most of the galaxy. The anomalously high number of WR stars means that we are actually witnessing a short period immediately after the last episode of star formation.

The central, brightest region, associated with this last star formation episode, is located in the south-eastern part of the galaxy and includes the largest and densest HI cloud, a molecular cloud seen in CO lines, a conspicuous dust lane, and a complex of large emission nebulae, reaching 300–400 pc

in size, with two shell nebulae HL111 and HL106 (according to the catalog of Hodge & Lee [20]), as well as young star clusters and about a dozen WR stars (see [8, 9, 10, 5, 7] and references therein). An $H\alpha$ image of this central region of the galaxy is shown in Figure 1.

According to Vacca et al. [16], the center of the last star formation episode is located near the object that was earlier classified as the WR star M24. (Hereafter letters R and M, followed by a number, refer to WR stars from the lists of Royer et al. [22] and Massey & Holmes [18], respectively). Vacca et al. [16] showed that M24 is actually a close group consisting of at least six blue stars, four of these stars being possible WR candidates. Lopez-Sanchez et al. [23] have conclusively identified two WR stars in this region. The HL111c nebula, surrounding M24, is one of the brightest HII regions in IC 10 and the brightest part of the HL111 shell. The neighborhood of M24 and the inner cavern of this shell host youngest (2–4 Myr old) star clusters in the galaxy [7, 14].

The shell nebula HL106 is located in the densest southern part of a complex, consisting of HI, CO, and dust clouds mentioned above. The ionizing radiation in this region must be generated by WR stars R2 and R10 and clusters 4-3 and 4-4 from the list of Hunter [14]. According to the above author, these clusters are a few times older than young clusters 4-1 and 4-2 in the HL111 region.

From the south, adjacent to the HI and CO clouds and the dust lane is a unique object, the so-called synchrotron supershell [24]. Until recently, it was believed to have been formed as a result of multiple explosions of about a dozen supernovae [24, 25, 26, 27]. Lozinskaya & Moiseev [28] for the first time explained the formation of this synchrotron supershell by a hypernova explosion.

The above features of IC 10 offer great possibilities for the study of the structure and physical characteristics of the dust component of a dwarf galaxy and the role that shocks play in its evolution. In this paper we analyze the connection between our data on IC 10, obtained earlier, and observations of this galaxy with the Spitzer telescope. In the following sections we describe the technique used to analyze these observations, present the obtained results and discuss them. In Conclusions we summarize the main findings of this work.

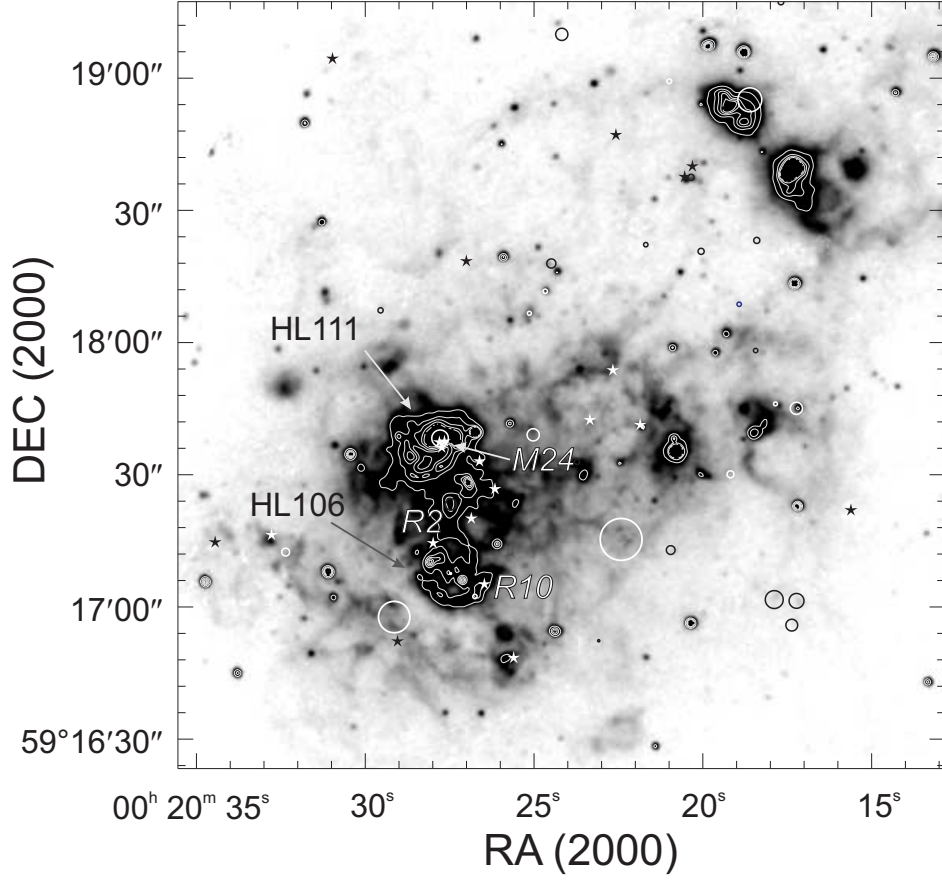


Figure 1: An $H\alpha$ image of the central region of the IC 10 galaxy with the contours showing regions of high $H\alpha$ intensity. The asterisks and circles show WR stars and clusters from the list of Tikhonov & Galazutdinova [21], respectively. HL111 and HL106 regions, mentioned in the text, are also indicated along with stars WR M24, R2, and R10.

2 Observations

2.1 IR observations

In this paper we use Spitzer archive observations of IC 10 obtained as a part of the program “A mid-IR Hubble atlas of galaxies” [29]. These data were downloaded from the Spitzer Heritage Archive¹. The MOPEX software² was utilized to compose image mosaics and custom IDL procedures were used to analyze them.

One of the most complicated issues in the analysis of such images is the choice of the background level. Sandstrom et al. [3] used a rather sophisticated procedure for this purpose, because the Small Magellanic Cloud occupies a large area on the sky. The angular size of IC 10 is small and one may therefore expect that background (mostly intragalactic and zodiacal) variations are small toward this galaxy. In this paper we set the background level in all the IR bands considered to the average brightness in areas located far from the star forming regions in IC 10. The adopted background values are listed Table 1. Such a simple procedure for background estimation is acceptable for our purposes. It is interesting that background values estimated using SPOT (Spitzer Planning Observations Tool), which are also shown in Table 1 (these are values written in FITS file headers), in some cases differ appreciably from the adopted values. This further supports the use of the background estimate extracted from real data.

2.2 Optical and 21 cm line observations

To analyze possible effects of shocks on the dust component, we use results of $H\alpha$ and $[SII]\lambda 6717\text{\AA}$ observations, made with the SCORPIO focal reducer and the scanning Fabry-Perot interferometer at the 6-m telescope of the Special Astrophysical Observatory of the Russian Academy of Sciences and described in detail by Lozinskaya et al. [12] and Egorov et al. [30]. To compare the dust component distribution with the large-scale structure and kinematics of HI in IC 10, we used 21-cm VLA data obtained by Wilcots and Miller [8]. Egorov et al. [30] reanalyzed the data cube of these observations, provided to us by the authors, in order to study the “local” structure and kinematics of HI in the neighborhood of the star forming complex and the

¹<http://sha.ipac.caltech.edu>

²<http://ssc.spitzer.caltech.edu/dataanalysistools/tools/mopex/>

Table 1: IR background levels toward IC 10 adopted in this paper and background levels according to SPOT.

Passband	Adopted background level (MJy/sr)	Background level according to SPOT (MJy/sr)
3.6 μm	0.1	0.2
4.5 μm	0.1	0.4
5.8 μm	0.1	2.6
8.0 μm	4	12
24 μm	19	25
70 μm	30	28
160 μm	80	163

brightest nebulae HL111 and HL106. We used the data with an angular resolution of $4.7'' \times 5''$ (corresponding to a linear resolution of about 20 pc for the adopted distance of 800 pc to the galaxy).

3 Results

The IR and $\text{H}\alpha$ maps of the central region of IC 10 are shown in Figure 2. The interest to near-IR observations of galaxies is related to the fact that UV-excited PAH bands can be used as an indicator of the number of hot stars and hence as an indirect indicator of the star formation rate. Draine & Li [31] proposed to parameterize the UV radiation field of the galaxy as the sum of the “minimum” diffuse UV field U_{min} (the lower cutoff of the starlight intensity distribution), filling up most of the galaxy’s volume, and a more intense UV field with a power-law distribution, which illuminates only the mass fraction γ of all the dust in the galaxy. The U_{min} quantity, expressed in units of the average UV radiation field in our Galaxy, characterizes the overall rate of star formation in the system studied, whereas γ allows one to estimate the mass fraction of the galaxy involved in the ongoing star formation. Other parameters introduced are the 24-to-70 μm flux ratio, which characterizes the fraction of “hot” dust, and $f(U > 10^2)$, the dust luminosity fraction contributed by regions with the UV radiation intensity $U > 10^2$, i.e., the dust luminosity coming from photodissociation regions.

Draine & Li [31] proposed a general algorithm for estimating the parameters of a galaxy from IR observations at 8 μm , 24 μm , 70 μm , and 160 μm

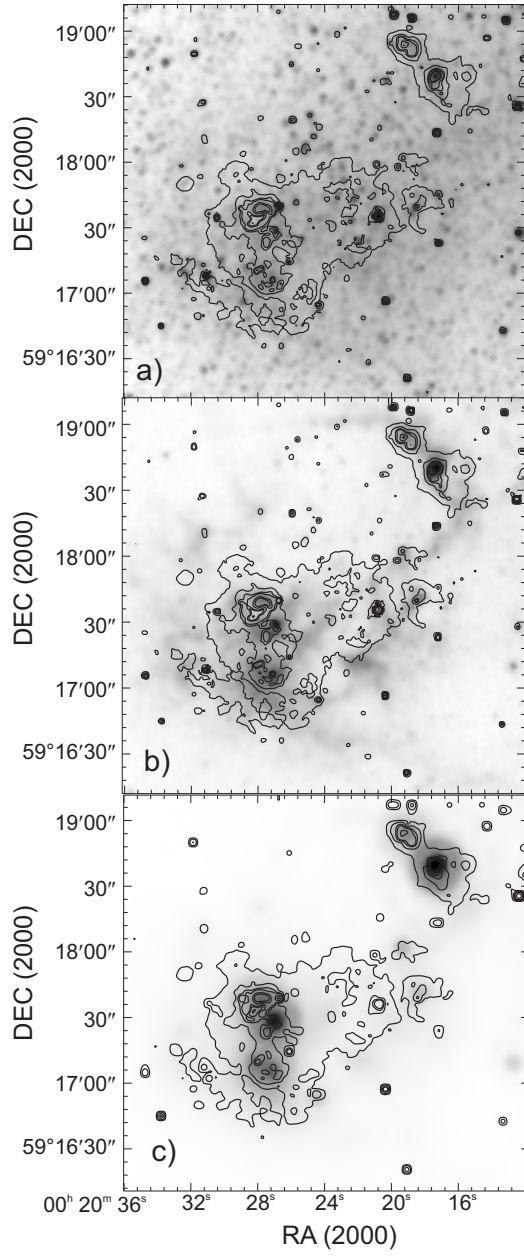


Figure 2: Maps of the central star forming region in IC 10 in different IR passbands: 3.6 μ m (the upper panel); 8 μ m (the middle panel), and 24 μ m (the lower panel). Superimposed on the maps are H α contours corresponding to the levels of 10^3 , $3 \cdot 10^3$, $7 \cdot 10^3$, 10^4 , $2 \cdot 10^4$, $3 \cdot 10^4$, 10^5 , $3 \cdot 10^5$, $5 \cdot 10^5$, $7 \cdot 10^5$, 10^6 , $2 \cdot 10^6$, and $3 \cdot 10^6$ in arbitrary units.

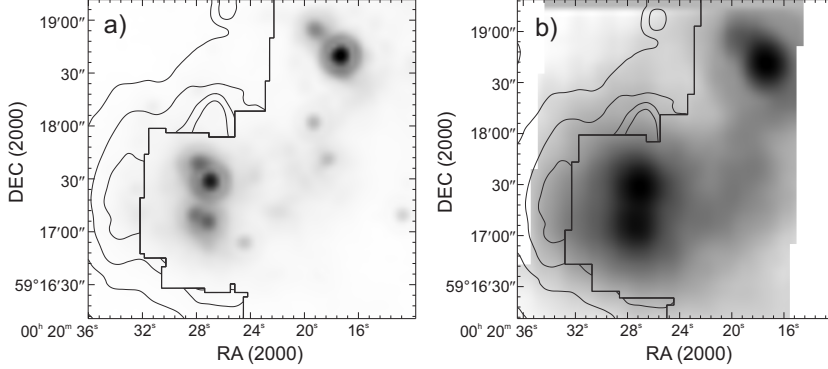


Figure 3: The 24 μm (left panel) and 70 μm (the right panel) maps of the central part of the star forming region in IC 10 with 160 μm emission contours.

(3.6 μm data are used to remove the starlight contribution). Unfortunately, this algorithm can be applied to IC 10 only partially, because 160 μm observations are not available for a substantial part of the galaxy. Results of long-wavelength observations are shown in Figure 3. As is evident from the figure, 160 μm data are mostly available for outskirts of the galaxy and cover the star forming regions only partially (taking into account the angular resolution, which is equal to 40'' at 160 μm).

Nevertheless, we used the available data and the technique described by Draine & Li [31] to determine U_{min} , γ , and q_{PAH} , the mass fraction of dust contained in PAH (or, more precisely, in particles with less than 1000 carbon atoms). We then averaged the data of IR observations over the region of IC 10, covered by 160 μm data, and inferred the following parameters for this region: $U_{\text{min}} = 20$, $\gamma = 0.04$, and $q_{\text{PAH}} = 3.9\%$. A comparison of these values with results of Draine et al. [4] for 65 galaxies of different types shows that parameters of IC 10 differ appreciably from the typical values of the corresponding quantities. Comparable U_{min} values are only found for two other Irr galaxies — NGC 2915 ($U_{\text{min}} = 10$) and NGC 5408 ($U_{\text{min}} = 20$). Note that NGC 5408 was also shown to contain starburst regions [32].

The γ parameter of IC 10 is also close to that of NGC 5408, but is much lower than the corresponding value in Mrk 33, another irregular galaxy from the list of Draine & Li [31], where it exceeds 10%. (Draine & Li [31] also report high γ value for the Seyfert galaxy NGC 5195, however, the result for this object is more dependent on the adopted radiation field parameters

than in the case of Mrk 33.) In the sample of Draine & Li [31] Mrk 33 is also the galaxy with the highest 24-to-70 μm flux ratio (~ 0.6) and the largest value of $f(U > 10^2) \approx 48\%$. The corresponding values for IC 10 are equal to about 0.7 and 23%, respectively. On the whole, as far as radiation-field parameters are concerned, IC 10 is quite a typical Irr starburst galaxy.

The IC 10 galaxy has unusually high PAH mass fraction q_{PAH} . Its value, inferred using the technique of Draine & Li [31], significantly exceeds the corresponding parameters for all the galaxies mentioned above (1.3% in Mrk 33, 2.4% in NGC 5195, 1.4% in NGC 2915, and 0.4% in NGC 5408). In the algorithm of Draine & Li [31] this parameter is inferred from the sole quantity—the ratio of the average 8 μm flux to the sum of the 70 μm and 160 μm fluxes. Our estimate for this parameter is 0.19, which, according to Draine & Li [31], corresponds to $q_{\text{PAH}} = 3.9\%$. To check whether such an unusually high q_{PAH} is obtained due to the lack of 160 μm data, we performed a more detailed fit of the observed 5.8 μm , 8 μm , 24 μm , and 70 μm fluxes based on the models of Draine & Li [31] using local rather than average fluxes. This technique allowed us to obtain individual estimates for different regions of the galaxy. Our modeling showed that the final average q_{PAH} and its distribution across the galaxy do depend appreciably on the choice of the passbands used in the fit. However, all the considered cases still yield a high 8 μm flux-averaged PAH fraction ranging from 2.9% to 4.5%. Note that the distribution of q_{PAH} in the galaxy is quite irregular. Along with regions of high q_{PAH} there are vast areas, where q_{PAH} is less than 1%.

As we mentioned above, the particular features of the distribution of q_{PAH} depend on the choice of passbands used in the fit of photometric data. Hereafter we use the 8 μm to 24 μm (F_8/F_{24}) flux ratio as the local indicator of the PAH fraction. A number of authors and, in particular, Sandstrom et al. [3], pointed out the possibility of using the above flux ratio for this purpose (note, however, that the correlation between F_8/F_{24} and q_{PAH} found by Sandstrom et al. [3] is rather weak). The halftones in Figure 4 (left panel) show the distribution of this flux ratio in the central star forming region of IC 10, and contours correspond to the distribution of $\text{H}\alpha$ intensity. Lighter tones indicate low F_8/F_{24} ratios and, correspondingly, low q_{PAH} , whereas darker tones indicate higher q_{PAH} . A wide semi-ring near the HL111 and HL106 regions is immediately apparent, which can be traced by low F_8/F_{24} ratio, weak $\text{H}\alpha$ intensity, and the locations of WR stars (we connected them by lines to emphasize the location of the semi-ring). It might be supposed that the low PAH abundance in this region is caused by the destruction of

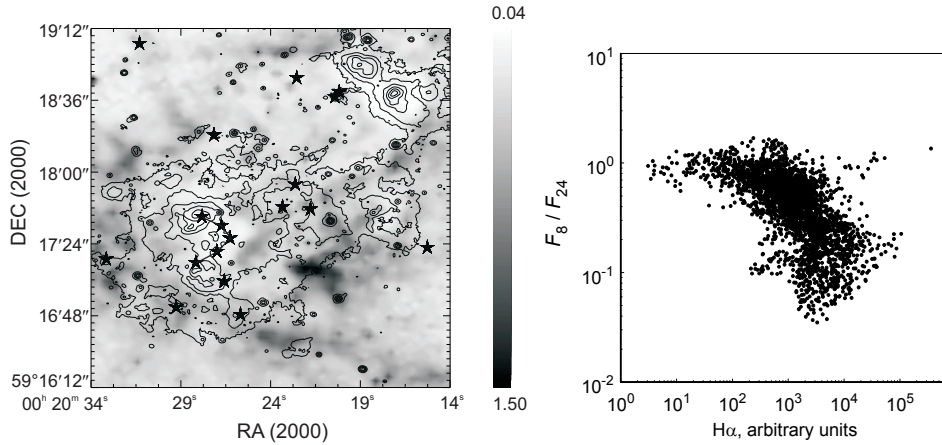


Figure 4: Left panel: the distribution of F_8/F_{24} flux ratio in the central star forming region of IC 10. Lighter tones correspond to lower flux ratios. Also shown are $H\alpha$ contours. Asterisks indicate positions of WR stars. Right panel: the correlation between the F_8/F_{24} flux ratio and $H\alpha$ intensity for the region shown in the left panel; only data points where $8\ \mu\text{m}$ flux exceeds 5 MJy/sr are included in the plot.

these particles by the ultraviolet radiation of WR stars, however, further studies are needed for a more definite conclusion.

The relation between the PAH abundance and star formation tracers is apparent not only in this semi-ring, but in the entire considered region. In the right panel of Figure 4 we show the correlation between the F_8/F_{24} flux ratio and $H\alpha$ intensity. It is evident from the figure that F_8/F_{24} (and hence q_{PAH}) decreases with increasing $H\alpha$ intensity. This may indicate that factors operating in the vicinity of the region of ongoing star formation, e.g., the UV radiation, have a destructive effect on PAH particles. The F_8/F_{24} flux ratio approaches unity in regions with less intense $H\alpha$ flux, and this corresponds to q_{PAH} values of about 2–3% [3].

PAH particles may also be destroyed by shocks. Therefore, generally speaking, the above-mentioned low F_8/F_{24} -ratio “semi-ring” located near HL111 and HL106 might have formed due to the destructive effect not only from the UV radiation of the WR stars located within it, but also from shocks produced by winds of these stars.

The primary shock indicators are high-velocity gas motions. A detailed study of the ionized gas kinematics in IC 10 by Egorov et al. [30] indeed

revealed weak high-velocity features in wings of $H\alpha$ and $[SII]\lambda 6717\text{\AA}$ lines in the inner cavern of the HL111 nebula and in other regions of the complex of violent star formation. In particular, such features were found in the vicinity of two WR stars located in the “semi-ring” mentioned above. We reanalyzed the results of observations of the galaxy in both lines made with the Fabry–Perot interferometer at the 6-m telescope of the Special Astrophysical Observatory of the Russian Academy of Sciences in order to reveal possible anticorrelation between high-velocity gas motions and q_{PAH} . We computed $H\alpha$ and $[SII]\lambda 6717\text{\AA}$ line profiles for several regions of high and low F_8/F_{24} ratio. Weak high-velocity features at a level of about 2–6% of the peak intensity are found in wings of both lines, and this coincidence confirms the reality of corresponding motions. However, these high-velocity features show up both in regions with high and low F_8/F_{24} ratios.

To obtain more definitive results, we mapped the distributions of velocities and intensities of high-velocity features in blue and red wings of $H\alpha$ line in the entire available field of the galaxy and in the central star forming region. The resulting maps indicate that high-velocity features in blue and red wings of the line show up in ranges from 50–60 to 100–110 km/s and 50 to 100 km/s, respectively, relative to the velocity of the line peak.

In Figure 5 we compare the F_8/F_{24} flux ratio to the intensities of high-velocity features in blue (left panel) and red (right panel) wings of $H\alpha$ line. If the PAH abundance depends on the presence of shocks, one would expect the intensity of high-velocity features to anticorrelate with F_8/F_{24} . No such anticorrelation can be seen in the figure, albeit a certain pattern does emerge: higher intensities of high-velocity features in both the blue and red wings tend to “avoid” regions with the highest F_8/F_{24} ratios, although they are observed in nearby, slightly offset, locations. Nonetheless, the results reported here do not allow us to conclusively associate the destruction of PAH particles with shocks produced by stellar winds and/or supernova explosions.

Arkhipova et al. [7] determined metallicities for a number of HII regions in IC 10. It is interesting to relate these metallicities to PAH content in order to see whether q_{PAH} decreases with decreasing metallicity within the galaxy in the same way as it does when we compare different Irr galaxies. Figure 6 shows the F_8/F_{24} ratios as a function of oxygen abundance for HII regions from the list of Arkhipova et al. [7]. In some cases two data points in this plot correspond to the same HII region. Metallicities of these HII regions inferred from long-slit and MPFS observations differ slightly, possibly due to different integration areas. We show only the data points with metallicity

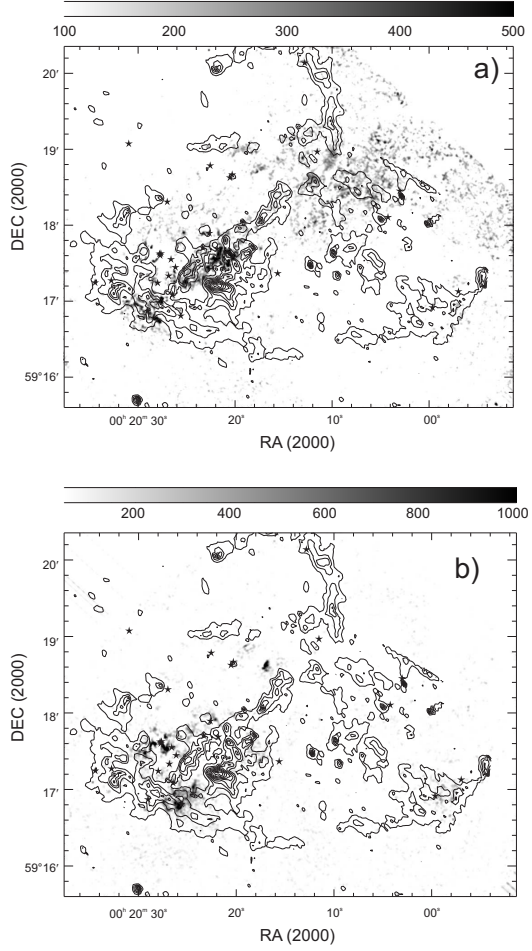


Figure 5: Intensity of blue (a) and red (b) wings of H α line with the F_8/F_{24} flux ratio contours superimposed.

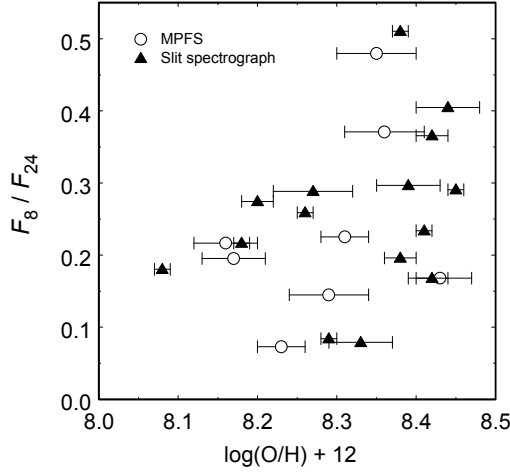


Figure 6: The F_8/F_{24} flux ratio toward HII regions from the list of Arkhipova et al. [7] as a function of oxygen abundance.

errors smaller than or equal to 0.05 dex.

It is evident from Figure 6 that the F_8/F_{24} ratio indeed decreases with decreasing oxygen abundance, although the turn-off value of $O/H + 12$ is about ~ 8.3 rather than $8.0-8.1$ as found in earlier works. This result indicates that the metallicity dependence of the PAH abundance shows up not only globally (at the level of entire galaxies), but also locally (at least at the level of individual HII regions).

As we pointed out in the Introduction, the only important difference between the two nearest Irr galaxies IC 10 and SMC is that in IC 10 we observe the interstellar medium immediately after a violent burst of star formation that has encompassed most of the galaxy. It is therefore of interest to compare the data obtained in this work with results of a detailed study of the dust component in the SMC performed by Sandstrom et al. [3]. (Recall that we use the F_8/F_{24} flux ratio to measure the PAH mass fraction and draw our conclusions based on this ratio.)

IC 10, like the SMC, shows strong q_{PAH} variations from one region to another with PAH avoiding bright HII regions. The lower spatial resolution prevents us from concluding that PAHs are located in the shells of bright nebulae, however, the large-scale map (Figure 4) shows clearly that the H_α brightness anticorrelates with the F_8/F_{24} ratio.

Sandstrom et al. [3] found weak or no correlation between q_{PAH} and

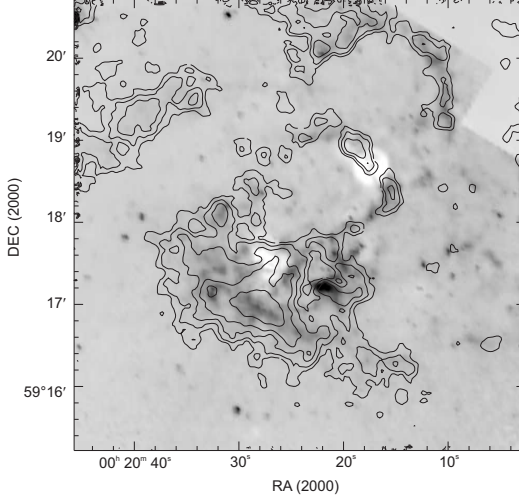


Figure 7: Map of the F_8/F_{24} flux ratio with HI emission contours superimposed.

the location of HI supershells in the SMC. The IC 10 galaxy, on the contrary, shows well-correlated (nearly coincident) extended shell-like structures in maps of F_8/F_{24} flux ratio and 21-cm HI emission (Figure 7). A correlation between the 8 μ m IR emission and the extended HI shell is also apparent in the middle panel of Figure 2.

The large-scale correlation between 8 μ m brightness and extended arcs and HII and HI shells in IC 10 and in a number of other starburst Irr galaxies has been known since long (Hunter et al. [33]). The above authors attributed all the 8 μ m flux solely to PAH emission and concluded that q_{PAH} correlates with brightness of giant shells and supershells. The correlation between the F_8/F_{24} flux ratio and the 21-cm line emission leads us to the same conclusion in a somewhat more straightforward way. We believe this is a real correlation, as the stellar wind from numerous young star clusters and WR stars located inside extended shells shapes observed shell-like structure of both the gas and dust in IC 10. Another implication is that PAH molecules do not undergo significant destruction during the sweep-up of giant shells (see also [33]).

The brightest extended CO cloud in the galaxy and the dust lane that coincides with it are located just to the south of the complex of ongoing star formation and are immediately adjacent to the HL106 nebula. Figure 8 shows the structure of this cloud according to data of Leroy et al. [10] superimposed

on the distribution of F_8/F_{24} flux ratio. (We obtained a composite map of the entire CO cloud by combining maps of its individual components: clouds B11a, B11b, B11c, and B11d in Figure 7 from [10].) The total gas column density $N(\text{HI})$ toward the dense cloud, discussed here, amounts to $\simeq 10^{22} \text{ cm}^{-2}$ [8]. According to CO emission observations, the column density of neutral and molecular hydrogen $N(\text{H})$ in this direction is about $2.8 \cdot 10^{22} \text{ cm}^{-2}$ [10, 34].

It follows from Figure 8 that three regions with highest F_8/F_{24} ratios have exactly the same locations and sizes as the CO clouds B11a, B11c, and B11d from [10]. The fourth CO cloud—B11b—coincides with the bright shell nebula HL106. Egorov et al. [30] showed that the optical nebula HL106 is not located behind a dense cloud layer, but is partly embedded in it. Egorov et al. [30] also concluded that B11b is physically associated with the optical nebula. First, the radial velocity of the B11b cloud ($V = -331 \text{ km/s}$ [10]) coincides with the velocity of ionized gas in HL106 determined by Egorov et al. [30]. But most importantly, the brightest southern arc HL106 exactly outlines the boundaries of the B11b cloud. Such an ideal coincidence cannot be accidental and hints to a physical relation between the thin ionized shell and the molecular cloud B11b. The HL106 shell, which exactly bounds the B11b cloud, formed due to photodissociation of molecular gas at the boundary of this cloud as well as due to ionization by the UV radiation of WR stars R2 and R10 and clusters 4-3 and 4-4. Hunter [14] estimates these clusters to be about 20-30 Myr old. The presence of a bright ionizing nebula that surrounds B11b explains low F_8/F_{24} flux ratio toward this cloud.

We can thus conclude with certainty that highest F_8/F_{24} ratios and, consequently, highest PAH fractions q_{PAH} are indeed found toward dense CO clouds. The only exception is the region of the brightest nebula HL45. The evident drop of the F_8/F_{24} flux ratio observed in this area may be due to destruction of PAHs by strong UV radiation.

4 Discussion and conclusions

In the Introduction we have already emphasized the importance of understanding the evolution of PAHs and their relation to other galaxy components. In this work we compare results of infrared observations of IC 10 with other available observations in order to identify possible indications to the origin of PAH.

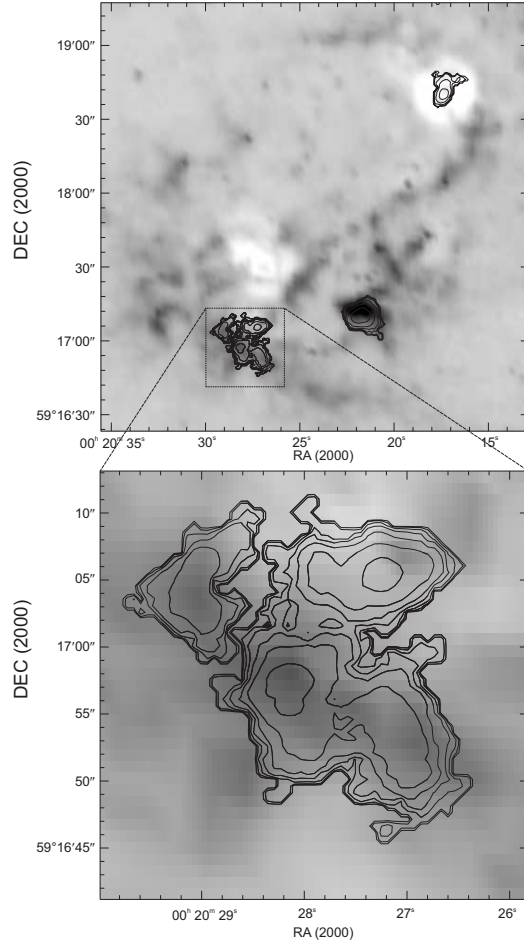


Figure 8: Map of F_8/F_{24} flux ratio with the contours of molecular gas distribution superimposed.

One of the key PAH properties to be explained by their evolutionary model is the low content of these particles in metal-poor galaxies. Two hypotheses are mainly discussed in the literature — less efficient formation and more efficient destruction of PAHs in metal-poor systems. Galliano et al. [35] argue that the dependence of q_{PAH} on the metallicity of a host galaxy can be naturally explained if we assume that PAH particles are synthesized in the atmospheres of long-lived AGB stars. In this case low metal and PAH abundances are due to the slower stellar evolution. However, if this assumption were true, the PAH fraction q_{PAH} in the IC 10 galaxy would be, first, low, and second, uniformly distributed throughout the galaxy. We show the pattern to be exactly the opposite — q_{PAH} (given by the F_8/F_{24} flux ratio) varies appreciably across the galaxy and amounts almost to 4% in some areas.

From the viewpoint of the spatial localization, PAHs correlate with both dense-gas indicators studied (HI and CO clouds). The PAH mass fraction decreases only in the neighborhood of HII regions and WR stars, which is consistent with the hypothesis that these particles are destroyed by UV radiation and shocks (although we failed to find convincing evidence for PAH destruction by shocks). On the whole, the pattern observed in IC 10 is qualitatively consistent with the assumption that PAH particles in molecular clouds form *in situ*. In this case the current high q_{PAH} value in IC 10 may be related to a recent burst of star formation during which PAH particles have formed in dense gas, and did not have enough time to be destroyed anywhere except for the immediate neighborhood of the UV radiation sources.

If this interpretation is correct, the metallicity dependence of q_{PAH} should show up until PAH particles begin to be destroyed by ultraviolet radiation, and reflects the peculiarities of their formation rather than their subsequent evolution. We further plan to verify our conclusions by analyzing observational results on other dwarf galaxies.

5 Acknowledgments

This work was supported by the Russian Foundation for Basic Research (grants nos. 10-02-00091 and 10-02-00231) and the Russian Federal Agency on Science and Innovation (contract no. 02.740.11.0247). O.V. Egorov thanks the Dynasty Foundation of Noncommercial Programs for financial support. Authors are grateful to Suzanne Madden and Tara Parkin for useful discus-

sions.

References

- [1] Tielens A.G.G.M. *Ann. Rev. Astron. Astroph.* **46**, 289 (2008)
- [2] Smith J.D.T., Draine B.T., Dale D.A., Moustakas J. et al. *Astrophys. J.* **656**, 770 (2007)
- [3] Sandstrom K.M., Bolatto A.D., Draine B., Bot C., Stanimirovic S. *Astrophys. J.* **715**, 701 (2010)
- [4] Draine B.T., Dale D.A., Bendo G. et al. *Astrophys. J.* **663**, 866 (2007)
- [5] Lozinskaya T.A., Egorov O.V., Moiseev A.V., Bizyaev D.V. *Astron. Lett.* **35**, 730 (2009)
- [6] Magrini L., Gonçalves D.R. *Mon. Not. Roy. Astron. Soc.* **398**, 280 (2009)
- [7] Arkhipova V.P., Egorov O.V., Lozinskaya T.A., Moiseev A.V. *Pis'ma Astron. Zh.* **37**, 83 (2011)
- [8] Wilcots E.M., Miller B.W. *Astron.J.* **116**, 2363 (1998)
- [9] Gil de Paz A., Madore B.F., Pevunova O. *Astrophys. J. Sup. Ser.* **147**, 29 (2003)
- [10] Leroy A., Bolatto A., Walter F., Blitz L. *Astrophys. J.* **643**, 825 (2006)
- [11] Chyzy K.T., Knapik J., Bomans D.J., Klein U., Beck R., Soida M., Urbanik M. *Astron. Astrophys.* **405**, 513 (2003)
- [12] Lozinskaya T.A., Moiseev A.V., Podorvanyuk N.Yu., Burenkov A.N. *Astron. Lett.* **34**, 217 (2008)
- [13] Richer M.G., Bullesjos A., Borissova J. et al. *Astron. Astrophys.* **370**, 34 (2001)
- [14] Hunter D. *Astrophys. J.* **559**, 225 (2001)
- [15] Massey P., Olsen K., Hodge P., Jacoby G., McNeill R., Smith R., Strong Sh. *Astron. J.* **133**, 2393 (2007)

- [16] Vacca W.D., Sheehy C.D., Graham J.R. *Astrophys. J.* **662**, 272 (2007)
- [17] Massey P., Armandroff T.E., Conti P.S. *Astron. J.* **103**, 1159 (1992)
- [18] Massey P., Holmes S. *Astrophys. J.* **580**, L35 (2002)
- [19] Crowther P.A, Drissen L., Abbott J.B., Royer P., Smartt S.J., *Astron. Astrophys.* **404**, 483 (2003)
- [20] Hodge P., Lee M.G. *Proc. Astron. Soc. Pacif.* **102**, 26 (1990)
- [21] Tikhonov N. A., Galazutdinova O. A. *Astron. Lett.* **35**, 748 (2009)
- [22] Royer P., Smartt S.J., Manfroid J., Vreux J. *Astron. Astrophys.* **366**, L1 (2001)
- [23] Lopez-Sanchez A.R., Mesa-Delgado A., Lopez-Martin L., Esteban C. *Mon. Not. Roy. Astron. Soc.* In press (arXiv:1010.1806)
- [24] Yang H., Skillman E.D. *Astron. J.* **106**, 1448 (1993)
- [25] Bullejos A., Rozado M. *Rev. Mex. (Ser de Conf.)* **12**, 254 (2002)
- [26] Rosado M., Valdez-Gutiérrez M., Bullejos A., Arias L., Georgiev L., Ambrocio-Cruz P., Borissova J., Kurtev R. *ASP Conf. Ser.* **282**, 50 (2002)
- [27] Thurow J.C., Wilcots E.M. *Astron. J.* **129**, 745 (2005)
- [28] Lozinskaya T.A., Moiseev A.V. *Mon. Not. Roy. Astron. Soc.* **381**, L26 (2007)
- [29] Fazio G., Pahre M. *Spitzer Proposal ID 69* (2004)
- [30] Egorov O.V., Lozinskaya T.A., Moiseev A.V. *Astron. Rep.* **87**, 277 (2010)
- [31] Draine, B.T., Li A. *Astrophys. J.* **657**, 810 (2007)
- [32] I. D. Karachentsev, M. E. Sharina, A. E. Dolphin, E. K. Grebel, D. Geisler, P. Guhathakurta, P. W. Hodge, V. E. Karachentseva, A. Sarajedini, P. Seitzer. *Astron. Astrophys.* **385**, 21 (2002)

- [33] Hunter D.H., Elmegreen B.G., Martin E. *Astron. J.* **132**, 801 (2006)
- [34] Bolatto A.D., Jackson J.M., Wilson C.D., Moriarty-Schieven G. *Astrophys. J.* **532**, 909 (2000)
- [35] Galliano F., Dwek E., Chianal P. *Astrophys. J.* **672**, 214 (2008)